A new theory for downslope windstorms and trapped mountain waves

François Lott
Laboratoire de Météorologie Dynamique, Ecole Normale Supérieure
24 rue Lhomond, 75231 Paris France, E-mail: flott@lmd.ens.fr

Journal of the Atmospheric Sciences: Accepted version of June 2016

Abstract

Linear mountain gravity waves forced by a nonlinear surface boundary condition are derived for a background wind that is null at the surface and increases smoothly to reach a constant value aloft and for a constant buoyancy frequency. In this configuration, the mountain waves have a critical level just below the surface which is dynamically controlled by the surface and minimum Richardson number J. When the flow is very stable ($J \gtrsim 1$), and when the depth over which dissipations act is smaller than the mountain height, this critical level dynamics easily produces large downslope winds and Foehn. The downslope winds are more intense when the stability increases and much less pronounced when it decreases (when J goes below 1). On the opposite, the trapped lee waves are very small when the flow is very stable, start to appear when $J \approx 1$ and can become pure trapped waves (e.g. not decaying downstream) when the flow is unstable (for $J < 0.25$). For the trapped waves, these results are explained by the fact that the critical level absorbs the gravity waves downstream of the ridge when $J > 0.25$, while absorption decreases when J approaches 0.25. Pure trapped lee waves follows that when $J < 0.25$ the absorption can become null in the non-dissipative limit. In the background flow profiles analysed, the pure trapped lee-waves also correspond to neutral modes of Kelvin-Helmholtz instability. The validity of the linear approximation used inflow is tested a posteriori by evaluating the relative amplitude of the neglected nonlinear terms.

1. Introduction

The interaction between mountains and synoptic meteorology can produce intense weather situations, like rotors and downslope winds that are very uncertain and quite difficult to predict (Doyle et al. 2009; Reinecke and Durran 2009). From a dynamical point of view, the difficulty is related to the fact that the gravity waves response to the mountain is extremely sensitive to the upstream flow conditions "near" the surface, where "near" means up to around the maximum mountain height. There, small changes in the background flow can yield large changes in the response (Georgelin and Lott 2001).

Two classical examples can be used to illustrate this sensitivity. The first is that mountain flow regimes are largely controlled by the non dimensional mountain height, $H_N = \frac{HN}{U_0}$, where H is the maximum altitude of the mountain, N the low level flow stability, and U_0 a scale for the low level incident wind (Smith 1979). It compares the vertical wavelength of the stationary gravity waves and the maximum mountain height. When the first is small compared to the second, the gravity waves break near aloft the mountain, and the resulting nonlinear dynamics can yield downslope windstorms and Foehn (see reviews by Smith (1985) and Durran (1990)). A problem is that it is hard to define N or U_0 when there are low level shears (Reinecke and Durran 2008): near the surface the vertical shear of the synoptic flow makes that the incident wind can become quite small and if the atmosphere is stable, H_N can be made arbitrarily large and extremely sensitive to small changes in the choice of U_0. From a dynamical point of view, this follows that the vertical wavelength of stationary gravity waves becomes small when the incident wind is small, e.g. it can almost always be made smaller than H by an appropriate choice. This near surface behavior is strongly reminiscent of the concept of critical level introduced by Booker and Bretherton (1967), and the fact that the surface can behave as a critical level for mountain waves was first noticed by Jiang et al. (2006). Importantly also, near a critical level, the horizontal winds due to the gravity waves can become very large. We will see that this can explain the onset of downslope winds and Foehn, even when there is no upper level gravity waves breaking.

The second example is that the low level shears control the onset of trapped waves, which are free modes of oscillations that are resonantly excited by mountains (Scorer (1949), see also the review in Durran (1990)). According to the conventional theory of trapped lee waves, these free modes develop along a low-level wave guide which can result either from (i) the trapping of vertically propagating solutions between a perfectly reflecting surface and a turning point aloft or from (ii) the free oscillation of a low level density discontinuity (for recent studies see Vosper (2004); Teixeira et al. (2013); Sachsperger et al. (2015)). Again, in most studies, the smallness of the incident wind near the surface and the presence of a wind shear above is not a central ingredient, except may be when the shear is confined to a relatively thin boundary layer.

The fact that there is a problem with the surface flow for mountain waves is not new, it has been addressed in numerical studies, who typically show that the boundary layer reduces the generation of mountain waves, eventually suppress gravity waves breaking aloft (Richard et al. 1989; Olafsson and Bougeault 1997; Peng and Thompson 2003), and dissipate trapped lee waves (Hills et al. 2016). Others emphasize the contribution of the boundary layer when there is more than one isolated mountain ridge (Stiperski

and Grubisic 2011), in the presence of surface heating (Smith and Skyllingstad 2011), and to the formation of lee rotors (Doyle and Durran 2002). Nevertheless, in these studies, free-slip boundary conditions or limited-slip conditions are often used near the surface, so the upstream wind does not go to zero at the surface, or decreases to near zero very rapidly (e.g. over few gridpoints). The two are nevertheless almost equivalent because few gridpoints cannot permit to solve well the near surface gravity waves dynamics. In these cases also, the wind shears are often confined to the boundary layer. In reality however, the vertical wind shears can extent up to the mid troposphere, as show the upstream profiles from Fig. 1 in Doyle et al. (2011) or Fig. 2 in Sheridan et al. (2007) observed in two distinct mountain waves field experiments. There are at least two mechanisms that can cause such a gradual increase of the wind with altitude. The first is that the incident wind is coming from very far upstream, so the boundary layer is fully developed. The second is that synoptic flows are primarily forced by thermal gradients that naturally produce vertical shears spanning few kilometers in depth. The impact of very small winds near the surface has not been much analyzed in the literature, at least from a conceptual point of view, and it can be assumed that in such flows the dynamics is essentially inviscid aloft, except near the surface where the absorption of gravity waves by a boundary layer needs to be taken into account.

The separation between an inviscid dynamics aloft interacting with a boundary layer is typically the approach followed by Smith et al. (2006) and Jiang et al. (2006) to explain why the conventional theories of trapped waves sometimes failed to explain observations (Smith et al. 2002). These papers analyze the reflection of the downward propagating waves by the boundary layer and discuss how it affects the low level wave-guide. They confront theories with simplified turbulent boundary layers and numerical simulations to show that more unstable boundary layers eventually support larger trapped waves.

It is in this context that Lott (2007) (hereinafter L07) calculates almost exactly the reflection of downward stationary gravity waves by a viscous boundary layer (e.g. the q-factor in Jiang et al. (2006)). In the viscous case, the wind at the surface has to be null, constant background wind shear and stratification are exact solutions, and L07 shows that the surface reflection decreases when the surface Richardson number J increases: perfect reflection only occurs in the inviscid limit when $J < 0.25$, suggesting again that unstable flows can give larger trapped waves (Smith et al. 2006). Note nevertheless that now the correspondence with stratified shear flow instability becomes very precise, the 0.25 value also being central in stratified shear flow stability theory (Miles 1961; Howard 1961). To support this further, L07 applies this result to evaluate the trapped solutions in a smooth $tanh$ background wind profile, e.g. a profile with an almost linear shear above $z = 0$, but where the wind becomes constant in $z \to \infty$. This is the profile used by Drazin (1958) to derive neutral modes of Kelvin-Helmholtz in the unbounded case. L07 found that when $J < 0.25$, the longest of the two modes identified Drazin (1958) can also be a trapped wave. With the necessary criteria $J < 0.25$ for perfect surface reflection, this example establishes an other strong relation between trapped waves and Kelvin-Helmholtz instabilities.

Basically, the purpose of this paper is to include a mountain forcing in the calculations of L07. Before doing so, it is worth to recall that there is a fundamental reason that makes this very involved: in the inviscid linear case, both (i) the vertical velocity associated with stationary gravity waves and (ii) the mountain forcing are null at $z = 0$. The inclusion of dissipations can help to circumvent the first problem, but as the viscous ones are extremely complex to treat, linear ones will be used next. Note also that from a more physical point of view, the use of dissipations is justified by the fact that dissipative effects ultimately control linear critical level dynamics (Booker and Bretherton 1967). For the second problem, a nonlinear free-slip boundary condition can be taken at $z = h$, the altitude of the mountain, rather than at $z = 0$ only (Long 1953).

The plan of the paper is as follows. The formalism is presented in section 2, results about downslope windstorms and Foehn are in section 3. Their sensitivity to J, the boundary layer depth, the maximum mountain height and their robustness against non-linear effects are in section 4. The results about trapped lee waves are in section 5. Section 6 concludes and discusses further the relations between trapped waves and instabilities. The Appendix derives the exact vertical structure of the monochromatic solutions used and some numerical issues to used to build the mountain wave field and some numerical issues.

2. Formalism and model

a. Basic equations

To analyze the mountain gravity waves produced by a stably stratified shear which is null at the surface, next consider the background flow profiles

$$U(z) = U_0 \tanh(z/d), N^2 = \text{constant}, \tag{1}$$

incident on a 2-dimensionnal mountain which height follows the Witch of Agnesi profile

$$h(x) = \frac{H}{1 + \frac{x^2}{2L^2}}. \tag{2}$$

In (1) $U(z)$ is the background horizontal wind, N the constant Brunt Vaisala frequency, z the altitude, d is the vertical scale of the shear and U_0 the incident wind maximum amplitude. In (2) H is the maximum mountain height, L its characteristic horizontal length, and x the horizontal coordinate. In the 2-dimensional non-rotating case the dynamics can be expressed with the non-dimensional variables:

$$\left(U, u', w'\right) = U_0 \left(\overline{U}, \overline{u}, \overline{w}\right), \; p' = \rho_r U_0^2 \overline{p}, \; b' = U_0 N \overline{b}, \; \left(x, z, h'\right) = \frac{U_0}{N} \left(\overline{x}, \overline{z}, \overline{h}\right), \tag{3}$$

where u' and w' are the disturbance horizontal and vertical velocities respectively, p' the pressure disturbance, b' the buoyancy disturbance, h' the surface elevation above $z=0$, and ρ_r a reference constant density. Then, assuming that inflow the disturbances produced by the mountain are small enough to be described by linear equations, the steady Boussinesq set describing them is:

$$\overline{U}\partial_{\overline{x}}\overline{u} + \overline{U}_{\overline{z}}\overline{w} + \partial_{\overline{x}}\overline{p} = -\overline{\epsilon}\,\overline{u} + \overline{\delta}^{-1}\partial^2_{\overline{x}}\overline{u}, \tag{4a}$$

$$\overline{U}\partial_{\overline{x}}\overline{w} + \partial_{\overline{z}}\overline{p} - \overline{b} = -\overline{\epsilon}\,\overline{w} + \overline{\delta}^{-1}\partial^2_{\overline{x}}\overline{w}, \tag{4b}$$

$$\overline{U}\partial_{\overline{x}}\overline{b} + \overline{w} = -\overline{\epsilon}\,\overline{b} + \overline{\delta}^{-1}\partial^2_{\overline{x}}\overline{b}, \tag{4c}$$

$$\partial_{\overline{x}}\overline{u} + \partial_{\overline{z}}\overline{w} = 0. \tag{4d}$$

This system will be forced by the non-linear free-slip boundary condition:

$$\overline{w}(\overline{x}, \overline{z} = \overline{h}) = \left(\overline{U}(\overline{h}) + \overline{u}(\overline{h})\right)\partial_{\overline{x}}\overline{h}. \tag{5}$$

In Eqs. (4)-(2) $\overline{U} = \tanh\left(\overline{z}/\sqrt{J}\right)$ and $\overline{h} = H_N/\left(1+\overline{x}^2/2F_r^2\right)$, where

$$J = \frac{N^2 d^2}{U_0^2},\ H_N = \frac{HN}{U_0},\ \text{ and } F_r = \frac{LN}{U_0} \tag{6}$$

are the surface and minimum Richardson number, the non-dimensional mountain height, and the Froude number respectively. These 3 parameters are central to our study, the significance of J and H_N have already been discussed in the introduction, whereas we know from the literature that the Froude number measures the significance of non-hydrostatic effects: when it decreases more harmonics are evanescent in the vertical when $z \to \infty$, and the relative contribution of the trapped harmonics to the total response increases.

The dissipative terms on the right hand sides of (4) are introduced to regularize the near surface critical level dynamics. They will always be small, the parameter $\overline{\epsilon} << 1$ being a Rayleigh drag in (4a)–(4b), and a Newtownian cooling in (4c). A viscous dissipation acting in the x-direction only is also used, it is characterized by the large "pseudo" Reynolds number $\overline{\delta} >> 1$. It is introduced because the Rayleigh drag alone is not efficient at large wavenumbers and to ensure that the model controls the linear critical level dynamics of all the harmonics. From a scale analysis of (4) we can tell that these dissipative terms will compare in amplitude to the advective terms for non-dimensional altitudes $\overline{z} \approx (\overline{\epsilon}F_r + \overline{\delta}^{-1}F_r^{-1})\sqrt{J}$. To measure the significance of the dissipation, we construct from this scaling a non-dimensional boundary layer depth

$$Z_B = 5\left(\overline{\epsilon}F_r + \overline{\delta}^{-1}F_r^{-1}\right)\sqrt{J}. \tag{7}$$

With this choice and above this level, the effect of the dissipations typically falls below 20% of that of the advection by the background wind.

b. Semi-theoretical model

In the following, the overlines will be dropped for conciseness. As the inflow solutions are linear they will be expressed in terms of Fourier transforms,

$$w(x,z) = \int_{-\infty}^{+\infty} w(k,z)e^{ikx}dk, \text{ where } \hat{w}(k,z) = \frac{1}{2\pi}\int_{-\infty}^{+\infty} w(x,z)e^{-ikx}d\overline{x} \tag{8}$$

the dissipative terms on the right hand sides of (4a), (4b) and (4c) transform into $-\left(\overline{\epsilon} + \overline{\delta}^{-1}\overline{k}^2\right)\left(\hat{u}, \hat{w} \text{ and } \hat{b}\right)$ respectively: they are linear in the z-direction, and the dissipative effects are significant over altitudes which compare to the characteristic length

$$z_k = (\epsilon k + k/\delta)\sqrt{J}. \tag{9}$$

Sufficiently far above the surface, e.g. where $z >> z_k$, $\hat{w}$ almost satisfies the inviscid Taylor Goldstein equation,

$$\frac{d^2\hat{w}}{dz^2} + \left(\underbrace{\frac{1}{U^2} + \frac{2(1-U^2)}{J}}_{S(z)} - k^2\right)\hat{w} = 0, \tag{10}$$

where $S(z)$ is the Scorer parameter. This equation has solutions that can be expressed in terms of Hypergeometric functions (see appendix for details), and to impose a realistic behavior in $z \to \infty$ a "canonical" solution $\hat{w}_c(k,z)$ is introduced. It corresponds to a unit amplitude exponentially decaying disturbance in $z \to \infty$:

$$\hat{w}_c = 2^{-m}U^{1/2+i\mu}(1-U^2)^{m/2}W_{2(1)} \underset{z\to\infty}{\approx} e^{-mz/\sqrt{J}}, \tag{11}$$

where

$$\mu = \sqrt{|J - \frac{1}{4}|} \text{ and } m = \sqrt{J}\sqrt{|k^2 - 1|}, \tag{12}$$

and where the expression for $W_{2(1)}$ in term of an hypergeometric function of argument $1-U^2$ is given in the Appendix (see Eq.(33)). In (12), when $1 - k^2 < 0$, the trapped decaying modes in $z \to \infty$ become propagating and m is changed in $-i$sign(k)m, where the $-sign(k)$ is to insure upward group speed. Also, when $J < \frac{1}{4}$, μ is changed in $i\mu$. Near the surface, $\hat{w}_c$ has the asymptotic behavior:

$$\hat{w}_c \approx a_1 z^{\frac{1}{2}-i\mu} + a_2 z^{\frac{1}{2}+i\mu}. \tag{13}$$

where a_1 and a_2 are complicated functions of m and μ (see Appendix).

Near $z = 0$, the dissipations can no longer be neglected, but at leading order the vertical structure equation

$$\frac{d^2\hat{w}_c}{d\tilde{z}^2} + \frac{J}{\tilde{z}^2}\hat{w}_c = 0, \text{ where } \tilde{z} = z - iz_k, \tag{14}$$

can be derived (Booker and Bretherton 1967). It has for solution:

$$\hat{w}_c \approx a_1 \tilde{z}^{\frac{1}{2}-i\mu} + a_2 \tilde{z}^{\frac{1}{2}+i\mu} \tag{15}$$

where a_1 and a_2 are as in (13) to ensure matching with the inviscid solution.

To satisfy the lower boundary condition (5), a solution is searched under the form

$$w(x,z) = \int_{-\infty}^{+\infty} f(k)\hat{w}_c(k,z)e^{ikx}dk, \tag{16}$$

near the ground it corresponds to vertical and horizontal velocities approximated by

$$w(x,z) \underset{z\to 0^+}{\approx} \int_{-\infty}^{+\infty} \left(a_1(k)\tilde{z}^{1/2-i\mu} + a_2(k)\tilde{z}^{1/2+i\mu}\right) f(k)e^{ikx}dk \tag{17a}$$

$$u(x,z) \underset{z\to 0^+}{\approx} \int_{-\infty}^{+\infty} i\frac{f(k)}{k}\left(a_1(k)(\frac{1}{2} - i\mu)\tilde{z}^{-1/2-i\mu} + a_2(k)(\frac{1}{2} + i\mu)\tilde{z}^{-1/2+i\mu}\right) e^{ikx}dk. \tag{17b}$$

Used in the boundary condition (5) these expressions permit to evaluate the amplitude of each harmonics, $f(k)$, by inversion of the integral equation,

$$\int_{-\infty}^{+\infty} \left\{ a_1(k)\tilde{h}^{-1/2-i\mu}\left(\tilde{h} - \frac{i}{k}\left(\frac{1}{2} - i\mu\right)\frac{dh}{dx}\right) + a_2(k)\tilde{h}^{-1/2+i\mu} \right.$$
$$\left. \left(\tilde{h} - \frac{i}{k}\left(\frac{1}{2} + i\mu\right)\frac{dh}{dx}\right)\right\} e^{ikx}f(k)dk = U(h)\frac{dh}{dx}, \tag{18}$$

where $\tilde{h}(x,k) = h(x) - iz_k$ (see Appendix for the numerical aspects).

3. Downslope windstorms, Foehn and low level wave breaking

a. Experimental setup

To expose how the model can predict downslope winds and Foehn without upper level wave breaking, consider in this section a mountain of moderate elevation, $H_N = 0.2$. To limit the contribution of the trapped waves, a quite broad mountain $F_r = 10 >> 1$ and a quite large Richardson number $J = 2$ are also considered. The damping parameters are $\epsilon = 3.10^{-4}$ and $\delta = 180$, values that make the boundary layer depth (7) much smaller than the non-dimensional mountain height, $Z_B = 0.025 << H_N$. Finally the model grid has an horizontal dimension of $D = 1000$ spanned by $M = 2048$ points. For these grid and disspations the dissipative scales of the harmonics verify $\max(z_k) \leq 0.02 << 1$.

To interpret the results, the wave field is also compared to that predicted by the same model with uniform incident wind $U = 1$, and which is the solution proposed in Long (1953) (see also Laprise and Peltier (1989)). The treatment of the nonlinear boundary condition is done as previously, the only change is now that the characteristic vertical velocity is very simple,

$$\hat{w}_c(k,z) = e^{-m(k)z/\sqrt{J}} \tag{19}$$

so the inversion (18) transforms into

$$\int_{-\infty}^{+\infty} e^{-m(k)h(x)}\left(1 + i\frac{m(k)}{\sqrt{J}k}\right)e^{ikx}f(k)dk = \frac{dh}{dx}. \tag{20}$$

In this case, there is no singularity at the surface and the dimensional results do not depend on the Richardson number: J only appears in Eqs. (19) and (20) because the same non-dimensional variables are retained.

b. Results

The vertical velocity fields produced by the obstacle in the case where U varies and where U is constant are shown in Figs. 1a and 1d respectively. Both fields have the characteristic structure of vertically propagating mountain gravity waves, the phase lines are tilted in the direction opposite to the incident wind, and the vertical wavenumbers are comparable for large $z > 1$. A first important difference is that when the incident wind varies with altitude, the wave field is essentially located on the downstream side of the mountain whereas it stays well located above the ridge when the incident wind is uniform. When the incident wind is uniform, it is known from the literature that this almost purely vertical propagation is related to the fact that the Froude number Fr is large (Queney 1948), which is also a situation for which the hydrostatic approximation applies. Therefore, it is tempting to interpret the downstream development in Fig. 1 as a non-hydrostatic effect but two things tell that it cannot be the case. The first is that when the hydrostatic approximation is made here (simply by changing m in (12) by $m = -isign(k)\sqrt{J}$) the wave field obtained is almost identical to that in Fig. 1a (not shown). The second simply follows that near the surface the term $\frac{1}{U^2}$ largely dominate the Scorer parameter in (10): the non-hydrostatic effects becomes even less significant near the surface than in the far-field. Therefore, the asymmetry in the response between the upstream and downstream side of the ridge is clearly a consequence of combining an incident wind that goes to zero when approaching the surface and a nonlinear lower boundary condition.

This asymmetry is even more remarkable on the horizontal wind disturbance near the surface and because for each harmonics the horizontal wind amplitude $\hat{u}$ varies in $\tilde{z}^{-1/2}$ rather than in $\tilde{z}^{1/2}$ for $\hat{w}$ (see Eqs. 17a and 17b). The consequences on the total wind vector near the surface are quite spectacular, with a very strong wind flowing downslope of the ridge, whereas the total wind upslope is quite small (see Fig. 1b). When the incident wind is uniform, the difference between the upslope and downslope winds are not as pronounced, at least when the non dimensional mountain height $H_N = 0.2$. In the uniform incident wind case, one needs to go to much higher elevations to see a pronounced downslope/upslope asymmetry, e.g. for values $H_N \approx 1$ when breaking aloft starts (this is the configuration shown in Fig. 1e). Note also that when the incident wind varies, these strong downslope winds are much more confined along the mountain slope than when the incident wind is uniform (note the difference in vertical scales between Figs. 1b and 1e).

The upslope/downslope asymmetry is also very pronounced on the total buoyancy in Fig. 1c, where the Foehn effect is much more pronounced than in the uniform incident wind case (Fig. 1f). Note also that at the tip end of the downslope wind jet the flow becomes convectively unstable (see Fig. 1c near $x = 30, z = 1$), the buoyancy fields acquire a pattern strongly reminiscent of an hydraulic jump. Also and importantly, no wave breaking occurs aloft, and this is in strong contrast to the uniform incident wind case when $H_N = 1$ in Fig. 1f. In the uniform wind case wave breaking only occurs aloft the mountain, the Foehn effect downstream is not as pronounced as when the incident wind varies, and no convective overturning occurs on the lee-side of the mountain.

To emphasize that the model can predict downslope windstorms and Foehn much more systematically than when the incident flow is uniform, the two experiments in Fig. 1 have been repeated dividing the mountain height by a factor 2. The dissipations are divided by 2 as well, which leaves the ratio between the mountain height and the boundary layer depth Z_B unchanged. The results are in Fig. 2 and show, when the wind varies with altitude, almost the same results as in Fig. 1: a strong downslope wind in Fig. 2a, accompanied by a pronounced Foehn and convective instability at low level in the lee-side (Fig. 2b). These phenomena are almost absent or quite weak when the wind is uniform (Figs. 2c–2d).

4. Sensitivity tests and validity of the linear approximation

a. Sensitivity test

As suggested by the previous results, the intensity of the downslope winds predicted by the theory is somehow related to the relative amplitude between the mountain height and the boundary layer depth. It also depends on the Richardson number J, an issue that has not yet been shown. These sensitivities are next analysed more systematically by varying the Richardson number J, the mountain height H_N and the boundary layer depth Z_B. To measure the intensity of the response a measure of the amplitude of the downslope wind effect is defined as the ratio between the maximum of the horizontal wind disturbance along the foothills (define as the region with $z < H_N/2$ and $0 < x < 5F_r$) and the background wind at the top of the hill ($U(H/d)$):

$$\underset{\substack{z<H_N/2 \\ 0<x<5F_r}}{Max} \left(\frac{u(x,z)}{U(H/d)} \right). \tag{21}$$

Typically, when this factor approaches and exceeds 1, the dynamics induces along the foothill, wind amplitudes that compare and exceed the winds at the summit of the ridge. This measure of the amplitude that the dynamics produce intense downslope winds, is then calculated as a function of the penetration of the mountain into the shear $H/d = H_N/\sqrt{J}$, for 4 values of J, 6 values of Z_B and 6 values of H/d, e.g. an ensemble of 144 realisations. The results are in Fig. 3a and first show that the downslope winds become much more substantial when the flow becomes more and more stable. When $J = 0.5$ the downslope wind factor is always below 1, whatever is the boundary layer depth Z_B or the mountain height. When $J = 1$, the downslope wind factors stays limited around 1, again whatever are Z_B or H/d. When the flow become more stable, downslope winds start to become quite spectacular, the downslope wind factor reaching values up to 4 when $J = 1.5$ and when $Z_B = 0.01H_N$. This maximum value reaches more than 8 when $J = 2$. Off course in these extreme cases we cannot expect our model to stay valid (see next subsection), but it nevertheless tells that strong downslope winds are strongly favored in stable situations when $J > 1$.

The Fig. 3a also show an interesting sensitivity to the boundary layer depth. In general, and as soon as the flow stability permits (e.g. for $J > 1$ typically) there are strong downslope winds for boundary layer depth up to at least half the mountain height. Nevertheless the intensity of the downslope wind is clearly increasing when the boundary layer depth decreases. Finally, the results show a rather weak sensitivity to the penetration of the mountain into the shear H/d telling that downslope the disturbance winds are in general proportional to the background wind at the summit. It is the proportionality factor that is strongly sensitive, first to J and second to Z_B.

b. Amplitude of non-linearities

The predictions of downslope winds that have been done so far are obviously limited by the fact that the equations used inflow are linear. There is no theory that justifies this approximation in the presence of a nonlinear boundary, except when the incident flow is uniform (Long 1953). To see if some aspects of the model can nevertheless be trusted, it is possible to proceed a posteriori and to evaluate the error made when the nonlinear terms are neglected. For this purpose, the model can be used to evaluate the amplitude of the nonlinear advection term, e.g. the term $\|u\partial_x u + w\partial_z u\|$ if the analysis is on the horizontal momentum equation, and to compare it to the amplitude of the horizontal pressure gradient. To avoid divisions by zero, it is better to take for the later the amplitude of its associated complex form:

$$\left\| 2\int_0^\infty ik\hat{p}e^{ikx}dk \right\|. \tag{22}$$

The ratio between the two is shown in Figs. 3b,c, and d when $H_N = 0.2$, $Z_B = 0.05$ and for $J = 0.5$, 1, and 2 respectively. In the case $J = 0.5$ corresponding to weak downslope winds according to Fig. 3a, Fig. 3b shows that the nonlinear term is everywhere quite small. It reaches slightly more than 25% of the amplitude of the linear pressure gradient in a small region located near the surface along the foothill of the ridge. As expected, the nonlinear terms become more substantial when the downslope winds and Foehn intensify, e.g. for larger J's in Figs. 3c, and d. Still, and at least in the moderate downslope wind case in Fig. 3b, strong nonlinearities only occur in a small region, always located at low level, well downstream on the foothill. When the mountain height is changed these results stay essentially valid, the foothill and along slope domain where the nonlinear terms are significant increases with H_N, but not in a dramatic way compared to Figs. 3b–3d (not shown but this was tested up to $H/d = 0.5$). Finally, it is also likely that the changes produced by these nonlinear terms will affect the fluid essentially downstream of where the errors are located, the absolute group velocity of the gravity waves involved in the dynamics being essentially positive.

5. Trapped lee waves and low level shear flow stability

a. Theoretical prediction with linear dampings

According to L07, when $J > 0.25$, the stationary gravity waves propagating toward the ground are always absorbed, the absorbtion increasing when J increases. According to Jiang et al. (2006) this absorption makes that the trapped waves amplitude decays downstream. In the cases analysed here, this decay should therefore increases with J. When the flow is unstable, $J < 0.25$, L07 also shows that the absorption vanishes in the inviscid limit so "pure" (e.g. non decaying dowstream) trapped waves can exist. L07 also suggests that these pure trapped waves should correspond to the longest of the two neutral modes derived by (Drazin 1958). As the results in L07 are based on a viscous treatment of the boundary layer they are derived here for the case of a linear dissipation.

Fundamentally, it consists in finding if there exist harmonics that can satisfy the lower boundary condition $\hat{w}(z = 0) = 0$, and which can therefore be resonantly excited by the mountain. With linear dissipations, the condition $\hat{w}(z = 0) = 0$ imposes that the ratio q between the two solutions in (15) has amplitude

$$|q| = \left|\frac{a_2}{a_1}\right| = \left|(-iz_k)^{-2i\mu}\right|. \tag{23}$$

For $k > 0$ and in the inviscid limit $z_k \to 0$, this implies

$$|q| = e^{-\mu\pi} \text{ when } J > 0.25, \text{ and } |q| = 0, \text{ when } J < 0.25. \tag{24}$$

When $J > 0.25$ (24) suggest that the reflection $|q|$ increases when J increases. Nevertheless, as the identification between $|q|$ and reflection is only rigorously justified in the $J >> 1$ limit, a more precise measure of the absorption is given by the momentum flux. When $J > 0.25$ it is given by

$$\frac{\hat{u}\hat{w}^* + \hat{u}^*\hat{w}}{4} = \frac{\mu|a_1|^2}{2|k|}\left(1 - |q|^2\right), \tag{25}$$

and is always positive, which means that the downward propagating waves are absorbed. When $J < 0.25$, its amplitude

$$\left|\frac{\hat{u}\hat{w}^* + \hat{u}^*\hat{w}}{4}\right| = \frac{\mu|a_1|^2}{2|k|}\mathrm{Im}\left\{q\right\}, \tag{26}$$

and if (24) holds, when $J < 0.25$, $\mathrm{Im}\{q\} = 0$ as well: the ground reflection becomes total in the inviscid limit when the flow is unstable at the surface.

When the wind varies with altitude, partial or total reflections also occur aloft, and it is necessary to analyze if, in the presence of the subsequent multiple reflections, there are solutions that satisfy (24). To establish this, the Fig. 4a, shows the values of $|a_1|$ and $|a_2|$ as a function of $k > 0$ and corresponding to the canonical solution $\hat{w}_c(k, z)$ near the surface (13). The results are shown for different J, and when $J > 0.25$, $|a_2| \geq |a_1|$, so the condition (24) cannot be satisfied, because $e^{-\mu\pi} < 1$. Note in particular that for propagating modes (e.g. modes with $k < 1$, see (12)) $|a_2| > |a_1|$ whereas for trapped ones $|a_2| = |a_1|$ exactly. For $J < 0.25$, the situation for the propagating modes is now reversed since $|a_2| > |a_1|$ but $|a_2| \neq 0$ so the condition (24) can still not be satisfied. On the other hand, there are two points in the trapped sector that deserves attention, they are the points where $a_2 = 0$ and $a_1 = 0$. These two points correspond to the wavenumbers satisfying $J = k^2(1 - k^2)$, e.g. the wavenumbers of the neutral solutions of the unbounded problem found by Drazin (1958). For trapped waves, it is the first one that matters since it satisfies $|q| = 0$ in (24), it will next be shown that this neutral solution can become a pure trapped wave.

b. Model results

To treat more specifically the case of the trapped waves next are made simulations for a narrower mountain than in section 3 (e.g. for $Fr = 2$) and where J varies between 0 and 1. The contribution of the dissipations is also reduced by taking $Z_B = 0.005$. For completeness, the horizontal size of the domain now equals $D = 250$ and the number of horizontal gridpoints is still $M = 2048$.

The Fig. 4b shows the amplitude $|f(k)|$, characterizing the contribution of each harmonics to the wave field in (16). When $J < 0.25$ there is for each J a pronounced narrow peak exactly where $|a_2| = 0$. These peaks broaden when J becomes larger than 0.25 and almost disappear when J approaches 1. The responses on the vertical velocity fields are in Fig. 4c and displayed as a function of horizontal distance. As long as there are well defined pure trapped solutions, e.g. when $J < 0.25$, oscillations develop far downstream the ridge with little attenuation. These oscillations decay substantially with downstream distance when $J > 0.25$, but the transition is not brutal. For $J = 0.36$ and up to $J = 0.49$ in Fig. 4c, substantial trapped waves are present as far downstream as $x = 20$, e.g. an order of magnitude further than F_r. It is only when J approaches 1 that the disturbance stays entirely confined along the downstream flank of the mountain, and does not propagate downstream.

One important result in Fig. 4b is that the resonance for $f(k)$ when $J < 0.25$ occurs for trapped modes with k very near 1, which are modes that decay in the vertical very slowly according to (11) and (12). The consequences for the vertical velocity field are shown on Fig. 5a. It shows over the mountain a well defined vertically propagating wave, and in the lee well developed trapped waves, the lee waves amplitude being substantial up to $z = 4$, e.g. well above the low level shear zone. For larger values of J (Fig. 5b), the trapped modes become more confined at low level, because the now less pronounced maxima in $f(k)$ in Fig. 4b occurs for k-values substantially larger than 1. The Fig. 5c also show that the downstream development falls off rapidly when J becomes large.

As for the downslope windstorms in Section 3, the degree of nonlinearities of the response has been evaluated. As the Foehn effect is not very strong for the values of the Richardson number $J < 1$ considered, it is found that the relative importance of the nonlinearities can be controlled by the dissipative scale. For the trapped waves developing downstream, the nonlinear term become significant near the surface when the non dimensional mountain height is large compared to the boundary layer depth, as in the case in the examples shown in Figs. 4-5, somehow as predicted by nonlinear dissipative critical level theory (Lott and Teitelbaum 1992).

6. Discussion

In the midlatitudes, the synoptic scale flows produced by horizontal thermal gradients, or associated with low level fronts systematically present vertical wind shears. These shears extend from the surface where the wind is small to the mid or high troposphere where the westerly jet cores are located. Such increase of the wind with altitude can also correspond to a well developed boundary layers. Starting from well understood theoretical tools, like the inviscid theory of mountain waves and the theory of stratified shear flow instabilities, this paper has analysed the impact of these low level shears on mountain waves. The fact that a null background wind at the surface yields a degenerated problem in the inviscid linear case is solved by adding a small dissipation and by considering a nonlinear boundary condition.

The central result of the paper is that the critical level dynamics near the surface plays a crucial role in the response. It produces large horizontal wind and buoyancy disturbances at low level that result in intense downslope winds and Foehn. These phenomena occur almost systematically when the flow is stable ($J \gtrsim 1$), and when the boundary layer depth is smaller than the maximum mountain height. The downslope winds intensity also rapidly increases when the flow stability increases. This behavior is consistent with the fact that in nature downslope winds more likely occurs during night, e.g. during more statically stable situations (Jiang and Doyle 2008). Interestingly, the mechanism proposed here do not call for upper level wave breaking or trapped waves resonance as often suggest other theories (Smith 1985; Durran 1990). Note nevertheless that the purpose here is not to invalidate these theories, but rather to shown that an important ingredient is missing in them, the low level shear of the large scale winds. In fact, and to be complete, it should be kept in mind that strong downslope winds can occur without upper level wave breaking in the full 3D case (Miranda and James 1992), and that hydraulic theories of downslope winds have also revealed the significance of having incoming flows that are slow at low level (Winters and Armi 2014). Finally, it is also important to recall that in real flow, the wind shear can be very strong near the surface in fairly shallow layer and less intense aloft, the model presented here does not capture this.

The critical level dynamics also impacts the onset of trapped lee waves. Their downstream extension also becomes conditional to the value of the Richardson number at the surface, with trapped lee waves occurring more easily when $J < 1$ and decreases. The connection with shear flow stability is further supported by the fact that in our profiles, and when $J < 0.25$, some well known neutral modes of Kelvin-Helmholtz can become pure trapped mountain waves. Another more "historical" analogy is may be worthwhile to mention. In the early literature about Kelvin-Helmholtz instabilities, some authors have used discontinuous wind profiles and found that these profiles are unconditionally unstable (Lindzen 1974). This in fact does not contradict the Miles (1961)-Howard (1961) theorem since a jump in the wind in fact corresponds to a null Richardson number. In mountain wave theory, when the upper level wind just above the surface is finite, it should be considered that the Richardson number at the surface is null, because the wind exactly at the surface is null which yields an infinite surface shear. As found in many papers, the onset of trapped lee-waves in this case is no longer conditional to the low level shear flow stability. It was shown here that it becomes so when there is a finite shear at the surface. Such finite surface shears can well be more realistic than the infinite ones: they naturally occur when a fully developed boundary layer with a no-slip boundary condition is taken into account or when the incident flow is produced by thermal horizontal gradients.

The fact that inflow linear equations are not adapted when a nonlinear boundary condition is used has also been tested. In fact, from a theoretical point of view, Long (1953) only shows that such a combination is valid when the incident wind is uniform. Theory also shows that near critical levels, nonlinear effects can easily become significant, but also that their significance can be mitigated by dissipations (Lott and Teitelbaum 1992). These issue has been discussed by comparing the nonlinear contribution to the horizontal momentum equation $\vec{u} \cdot \vec{\nabla} u$ to the linear contribution of the pressure gradient $\partial_x p$. It was found that the first only dominates the second at the downstream foothills and when the downslope winds are strong, e.g. places where it is certain that the nonlinear effects will anyway affect the flow evolution. Upstream and aloft the ridge such a comparison shows that the linear hypothesis is essentially valid. Although this partially validate the model "a posteriori", the fact that in places nonlinearities become important now calls for further tests with full numerical models.

In this context some preliminary numerical results have shown that some of the results found are reproducible, and least when viscous disspations are included. The onset of downslope winds without upper level breaking when J is large seems robust, the onset of trapped lee waves when J becomes small also. These simulations also show that the transitionnal value $J = 1$ above which downslope winds easily occur and below which trapped waves start to be substantial can shift to larger values. For trapped waves, this is consistent with the viscous treatment in L07, the surface critical level absorptions being less intense with true viscosities than with the linear dampings used here.

Acknowledgments.

This work was supported by the European Commission's project ARISE2, (Grant agreement 653980). The author acknowledges Riwal Plougonven for helpful discussions and the three anonymous reviewers for their useful comments.

Appendix

Canonical solution: exact derivation and asymptotic properties

Taking $r = U^2 = \tanh^2(z/\sqrt{J})$, the Taylor-Goldstein Eq. (10) becomes

$$\frac{d^2\hat{w}}{dr^2} + \left(\frac{1}{2r} - \frac{1}{1-r}\right)\frac{d\hat{w}}{dr} + \left(\frac{J}{4r^2(1-r)^2} + \frac{1}{2r(1-r)} - \frac{k^2 J}{4r(1-r)^2}\right)\hat{w} = 0, \tag{27}$$

Equation (27) has three regular singular points, when $J - k^2 > 0$ its exponent pairs are:

$$r = 0: \quad \alpha_1 = \tfrac{1}{4} + i\tfrac{\mu}{2}, \quad \alpha_2 = \frac{1}{4} - i\frac{\mu}{2}; \tag{28}$$

$$r = 1: \quad \gamma_1 = -\tfrac{m}{2}, \quad \gamma_2 = +\frac{m}{2}; \tag{29}$$

$$r = \infty \quad \beta_1 = 1, \quad \beta_2 = -\frac{1}{2}, \tag{30}$$

μ and m being given by (12). Following Olver (1974), the change $\hat{w} = r^{\alpha_1}(1-r)^{\gamma_1} W$, (27) transforms into the Hypergeometric equation

$$r(1-r)\frac{d^2W}{dr^2} + \{c - (a+b+1)r\}\frac{dW}{dr} - abW = 0 \tag{31}$$

where

$$a = \alpha_1 + \beta_1 + \gamma_1 = \frac{5}{4} + i\frac{\mu}{2} - \frac{m}{2},\ b = \alpha_1 + \beta_2 + \gamma_1 = -\frac{1}{4} + i\frac{\mu}{2} - \frac{m}{2},\ c = 1 + \alpha_1 - \alpha_2 = 1 + i\mu. \tag{32}$$

To impose a realistic behavior in $z \to \infty$, the solution (15.5.6 in AS) is used:

$$W_{2(1)} = (1-r)^{c-a-b} F(c-b, c-a; c-a-b+1; 1-r), \tag{33}$$

where F is the Hypergeometric function, and the "canonical" solution in (11) that corresponds to a unit amplitude exponentially decaying disturbance in $z \to \infty$ (or to an upward propagating wave) is given by:

$$\hat{w}_c = 2^{-m} r^{\alpha_1} (1-r)^{\gamma_1} W_{2(1)}, \tag{34}$$

To evaluate $\hat{w}_c$ near the surface, the transformation (15.3.6 in AS) is used to express (33) in terms of the solutions (15.5.3 in AS) and (15.5.4 in AS), e.g.

$$W_{1(0)} = F(a,b;c;r) \text{ , and } W_{2(0)} = r^{1-c} F(a-c+1, b-c+1; 2-c; r) : \tag{35}$$

$$W_{1(0)} = A_1 W_{1(1)} + A_3 W_{2(1)},\ W_{2(0)} = A_2 W_{1(1)} + A_4 W_{2(1)} \tag{36}$$

where

$$A_1 = \frac{\Gamma(c)\Gamma(c-a-b)}{\Gamma(c-a)\Gamma(c-b)}, \qquad A_3 = \tfrac{\Gamma(c)\Gamma(a+b-c)}{\Gamma(a)\Gamma(b)},$$
$$A_2 = \frac{\Gamma(2-c)\Gamma(c-a-b)}{\Gamma(1-a)\Gamma(1-b)}, \quad A_4 = \tfrac{\Gamma(2-c)\Gamma(a+b-c)}{\Gamma(a-c+1)\Gamma(b-c+1)}. \tag{37}$$

This yields

$$\hat{w}_c = r^{\alpha_1}(1-r)^{\gamma_1} \left(b_1 W_{2(0)} + b_2 W_{1(0)} \right), \text{ where } b_j = (-1)^{j-1} \frac{2^{-m} A_j}{A_1 A_4 - A_2 A_3} \text{ for } j = 1, 4. \tag{38}$$

When approaching the surface, this inviscid solutions behaves as (13) providing that:

$$a_1 = b_1 J^{-1/4 + i\mu/2},\ a_2 = b_2 J^{-1/4 - i\mu/2} \tag{39}$$

Numerical aspects

To build a solution valid over the full domain a uniform approximation of the characteristic function, $w_c(k,z)$ is built by using the inviscid solution form in (11) when $z >> z_k$ and the damped solution (15) near $z = 0$. More precisely, a smooth transition is made between the two by using *tanh* vertical tapers centered on $z = 5z_k$ and of characteristic extension z_k. The other disturbance fields (e.g. $\hat{u}_c$ and $\hat{b}_c$) are obtained from the uniform approximation of $\hat{w}_c$ and using the the Fourier transforms of the Eqs. (4). Finally, and for the buoyancy b, the profiles are adjusted vertically in the physical space so that the predicted total buoyancy field is statically stable.

To evaluate the wave amplitude $f(k)$ in (16) the inversion of (18) is made numerically. More specifically, considering a domain of length D sampled by an odd-number M of points, the same horizontal wavenumbers and physical location as when fast Fourier transforms can be used, e.g., $k_j = (j-1)\frac{2\pi}{D}$ and $x_l = (l-1)\frac{D}{M}$, for j and $l = 1, M$. In this discrete formalism, (18) transforms into,

$$\sum_{j=1}^{M} W_{jl} f(k_j) = \left(U(h) \frac{dh}{dx} \right)_l, \tag{40}$$

where the matrix

$$W_{jl} = \frac{2\pi}{D} \left(a_{1j} \tilde{h}_{lj}^{-1/2 - i\mu} \left(\tilde{h}_{lj} - \frac{\frac{i}{2} + \mu}{k_j} \left(\frac{dh}{dx} \right)_l \right) + a_{2j} \tilde{h}_{lj}^{-1/2 + i\mu} \left(\tilde{h}_{lj} - \frac{\frac{i}{2} - \mu}{k_j} \left(\frac{dh}{dx} \right)_l \right) \right) e^{ik_j x_l}$$

Equation (40) is then solved by inverting the matrix W_{jl} with a conventional inversion software.

REFERENCES

Booker, J. R., and F. P. Bretherton, 1967: The critical layer for internal gravity waves in a shear flow. *J. Fluid Mech.*, **27**, 102–109, doi:http://dx.doi.org/10.1017/S0022112067000515.

Doyle, J. D., and D. D. Durran, 2002: The dynamics of mountain-wave induced rotors. *J. Atmos. Sci.*, **59**, 186–201.

Doyle, J. D., V. Grubisic, W. O. J. Brown, S. F. J. DeWekker, A. Dornbrack, Q. Jiang, S. D. Mayor, and M. Weissmann, 2009: Observations and numerical simulations of subrotor vortices during t-rex. *J. Atmos. Sci.*, **66**, 1229–1249, doi:http://dx.doi.org/10.1175/2008JAS2933.1.

Doyle, J. D., and Coauthors, 2011: An intercomparison of t-rex mountain-wave simulations and implications for mesoscale predictability. *Mon. Wea. Rev.*, **139**, 2811–2831, doi:http://dx.doi.org/10.1175/MWR-D-10-05042.a.

Drazin, P. G., 1958: The stability of a shear layer in an unbounded heterogeneous inviscid fluid. *J. Fluid Mech.*, **4**, 214–224, doi:http://dx.doi.org/10.1017/S0022112058000409.

Durran, D. R., 1990: Mountain waves and downslope winds. *AMS Meteorological Monographs*, **23**, 59–83.

Georgelin, M., and F. Lott, 2001: On the transfer of momentum by trapped lee waves. case of the iop3 of pyrex. *J. Atmos. Sci.*, **58**, 3563–3580.

Hills, M. O. G., D. R. Durran, and P. N. Blossey, 2016: The dissipation of trapped lee waves. part ii: the relative importance of the boundary layer and the stratopshere. *J. Atmos. Sci.*, **73**, 943–955, doi:10.1175/JAS-D-15-0175.1.

Howard, L. N., 1961: Note on a paper of john w miles. *J. Fluid Mech.*, **10**, 509–512.

Jiang, Q., and J. D. Doyle, 2008: On the diurnal variation of mountain waves. *J. Atmos. Sci.*, **65**, 1360–1377, doi:10.1175/2007JAS2460.1.

Jiang, Q., J. D. Doyle, and R. B. Smith, 2006: Interaction between trapped waves and boundary layers. *J. Atmos. Sci.*, **63**, 617–633, doi:http://dx.doi.org/10.1175/JAS3640.1.

Laprise, R., and W. R. Peltier, 1989: On the structural characteristics of steady finite-amplitude mountain waves over bell-shaped topography. *J. Atmos. Sci.*, **26**, 586–595.

Lindzen, R. S., 1974: Stability of helmholtz velocity profiles in a continuously stratified, infinite boussinesq fluid–applications to clear air turbulence. *J. Atmos. Sci.*, **31**, 1507–1514.

Long, R. R., 1953: Some aspects of the flow of stratified fluids; 1. a theoretical investigation. *Tellus*, **5**, 42–58.

Lott, F., 2007: The reflection of a stationary gravity wave by a viscous boundary layer. *J. Atmos. Sci.*, **139**, 3363–3371, doi:http://dx.doi.org/10.1175/JAS4020.1.

Lott, F., and H. Teitelbaum, 1992: Nonlinear dissipative critical level interaction in a stratified shear flow: instabilities and gravity waves. *Geoph. Astr. Fluid Dyn.*, **66**, 133–167.

Miles, J. W., 1961: On the stability of heterogeneous shear flow. *J. Fluid. Mech.*, **10**, 496–508.

Miranda, P. M. A., and I. N. James, 1992: *Quart. J. Roy. Meteor. Soc.*, **118**, 1057–1081.

Olafsson, H., and P. Bougeault, 1997: The effect of rotation and surface friction on orographic drag. *J. Atmos. Sci.*, **54**, 193–210.

Olver, F. W. J., 1974: Asymptotics and special functions. *Academic Press*, 572pp.

Peng, M., and W. T. Thompson, 2003: Some aspects of the effect of surface friction on flows over mountains. *Quart. J. Roy. Meteor. Soc.*, **129**, 2527–2558.

Queney, P., 1948: The problem of airflow over mountains: a summary of theoretical studies. *Bull. Amer. Meteor. Soc.*, **29**, 16–26.

Reinecke, P. A., and D. R. Durran, 2008: Estimating topographic blocking using a froude number when the static stability is non-uniform. *J. Atmos. Sci.*, **65**, 1035–1048, doi:10.1175/2007JAS2100.1.

Reinecke, P. A., and D. R. Durran, 2009: Initial-condition sensitivities and the predictability of downslope winds. *J. Atmos. Sci.*, **66**, 3401–3418, doi:http://dx.doi.org/10.1175/2009JAS3023.1.

Richard, E., P. Mascart, and E. C. Nickerson, 1989: The role of surface friction in downslope windstorms. *J. Appl. Meteor.*, **28**, 241–251.

Sachsperger, J., S. Serafinixi, and V. Grubisic, 2015: Lee waves on the boundary-layer inversion. *Frontiers in Geophysics*, Submitted.

Scorer, R. S., 1949: Theory of waves in the lee of mountains. *Quart. J. Roy. Meteor. Soc.*, **75**, 41–56.

Sheridan, P. F., V. Horlacherxi, G. G. Rooney, P. Hignett, S. D. Mobbs, and S. Vosper, 2007: Influence of lee waves on the near surface flow downwind of the pennines. *Quart. J. Roy. Meteor. Soc.*, **133**, 1353–1369, doi:10.100a/2qj.110.

Smith, C. M., and E. D. Skyllingstad, 2011: Effects of inversion height and surface heat flux on downslope windstorms. *Mon. Wea. Rev.*, **139**, 3750–3764, doi:http://dx.doi.org/10.1175/2011MWR3619.1.

Smith, R. B., 1979: The influence of mountains on the atmosphere. *Advances in Geophys.*, **21**, 87–230.

Smith, R. B., 1985: On severe downslope winds. *J. Atmos. Sci.*, **42**, 2597–2603, doi:http://dx.doi.org/10.1175/1520-0469(1985)042⟨2597:OSDW⟩2.0.CO;2.

Smith, R. B., Q. Jiang, and J. D. Doyle, 2006: A theory of gravity wave absorption by a boundary layer. *J. Atmos. Sci.*, **63**, 774–781, doi:http://dx.doi.org/10.1175/JAS3631.1.

Smith, R. B., S. Skubis, J. D. Doyle, A. S. Broad, C. Kiemle, and H. Volkert, 2002: Mountain waves over the mont blanc: Influence of a stagnant boundary layer. *J. Atmos. Sci.*, **59**, 2073–2092.

Stiperski, I., and V. Grubisic, 2011: Trapped lee wave interference in the presence of surface friction. *J. Atmos. Sci.*, **68**, 918–936, doi:http://dx.doi.org/10.1175/2010JAS3495.1.

Teixeira, M. A., J. L. Argain, and P. M. A. Miranda, 2013: Orographic drag associated with lee waves trapped at an inversion. *J. Atmos. Sci.*, **70**, 2930–2947, doi:10.1175/JAS-D-12-0350.1.

Vosper, S. B., 2004: Inversion effects on mountain lee waves. *Quart. J. Roy. Meteor. Soc.*, **130**, 1723–1748, doi:10.1256/qj.03.63.

Winters, K. B., and L. Armi, 2014: Topographic control of stratified flows: upstream jets, blocking and isolating layers. *J. Fluid. Mech.*, **753**, 80–103, doi:10.1017/jfm.2014.363.

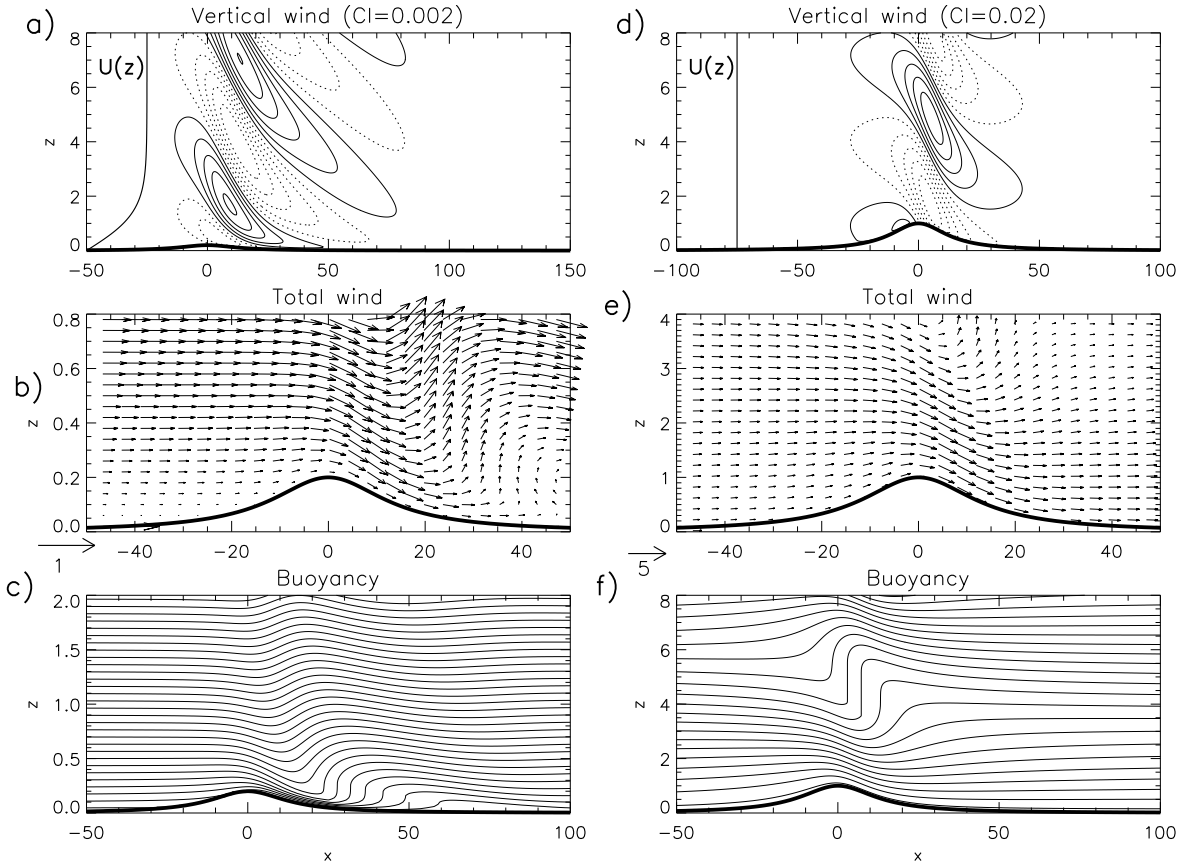

FIG. 1. Flow response for a mountain profile given by a "Witch of Agnesi", $h(x) = \frac{H_N}{1+\frac{x^2}{2F_r^2}}$, when $J = 2$, $Fr = 10$. When the incident wind varies (left column), $H_{ND} = 0.2$, when it is constant (right column) $H_{ND} = 1$. a) and d) vertical velocity; b) and e) total wind $(U + u, w)$; c) and f) total buoyancy: $z + b$.

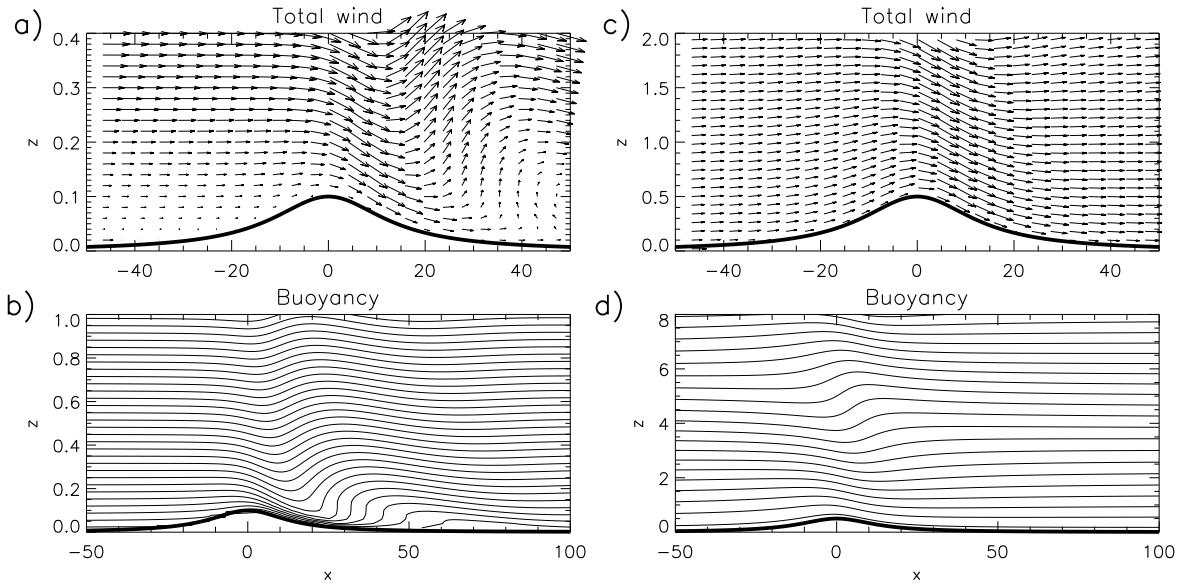

FIG. 2. Same as Figure 1 but for twice smaller mountains and dissipations.a) and c) total wind $(U+u, w)$; b) and d) total buoyancy: $z+b$.

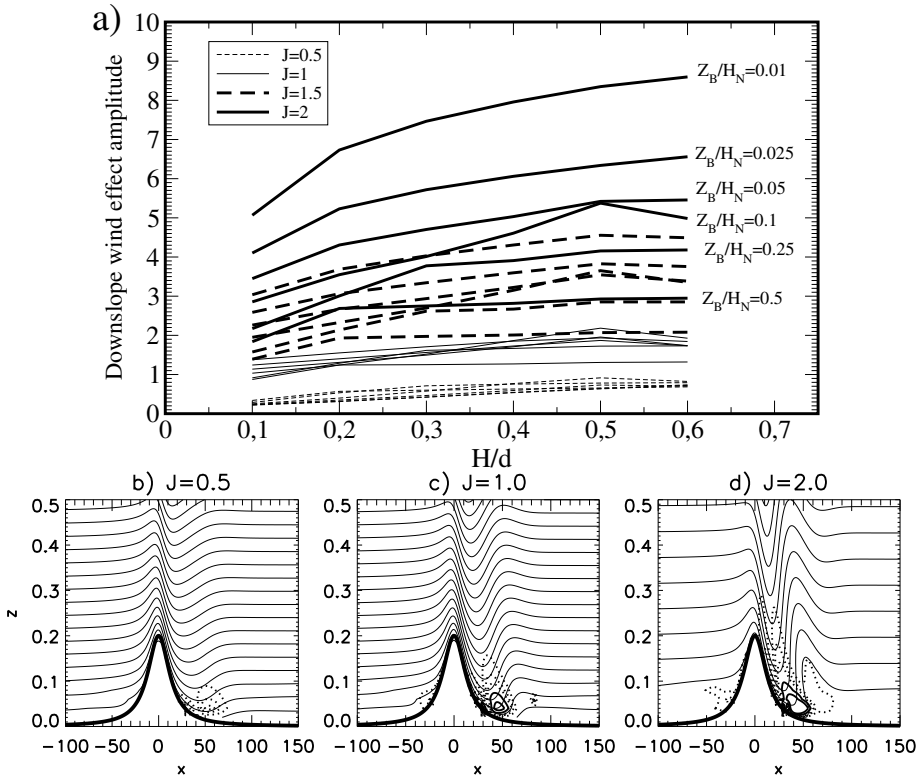

FIG. 3. Sensitivity tests and nonlinear effects: a) amplitude of the downslope wind effect as defined by (21). For clarity the various values of the ratio Z_B/H_N are only indicated for the cases with $J=2$. b) c) and d) streamfunction (thin solid) and nonlinear error defined by $\|u\partial_x u + w\partial_z u\| \,/\, \left\|2\int_0^\infty ik\hat{p}e^{ikx}dk\right\|$ for $J=0.5, 1$, and 2 respectively (the thick lines correspond to the contours=0.25, 0.5, 0.75, 1.25, 2, 5, the values below 1 are dashed).

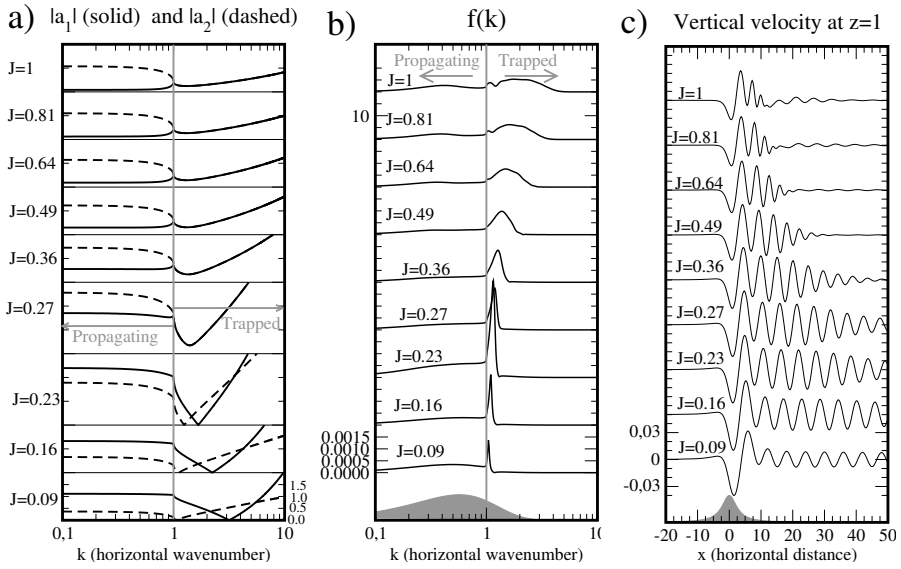

FIG. 4. a) Amplitude $|a_1(k)|$ and $|a_2(k)|$ of the parameters entering in the near surface solution (13), b) amplitude $|f(k)|$ attributed to each harmonics in (16) for a "Witch of Agnesi" profile $h(x) = \frac{H_N}{1+\frac{x^2}{2F_r^2}}$, where $H_N = 0.2$ and $F_r = 2$; and c) vertical velocity as a function of horizontal distance w and at $z = 1km$. In all panels, the various curves are shifted vertically for clarity and the zero lines are shown in a).

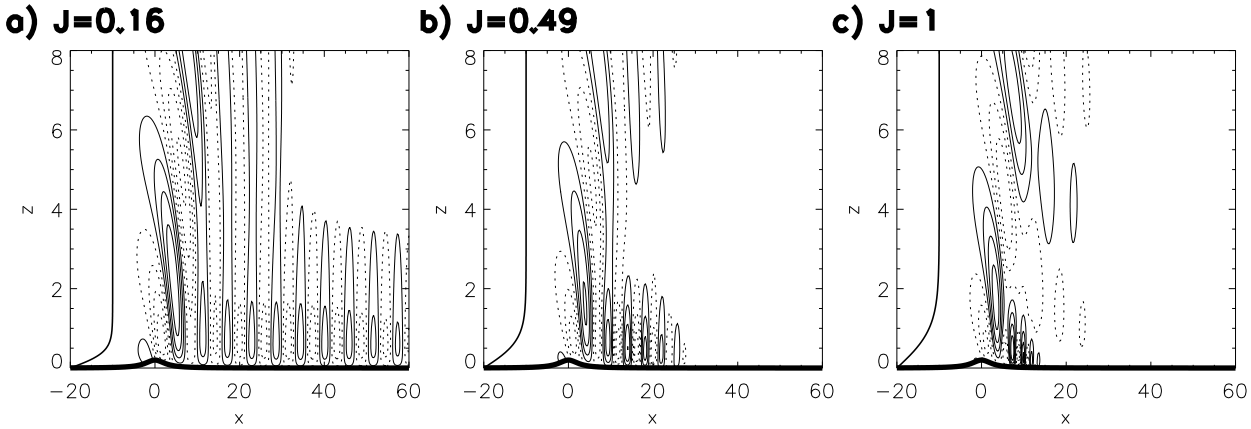

FIG. 5. Vertical velocity fields for various values of the Richardon number J. The background wind profile $U(z)$ is in bold and the contour interval for w is 0.01. Same parameters as in Fig. 4